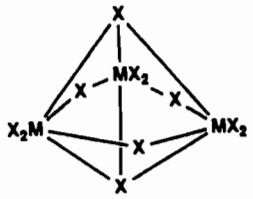

B

the coordination sphere of three metals. The Ce_4O core reported here is clearly related to the M_3X_{11} motif by the grafting of a fourth MX_3 unit onto the M_3X_{11} core to form a wingtip of the butterfly (see C, where dashed lines indicate newly formed bonds).

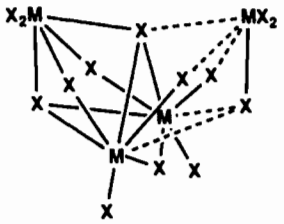

C

The coordination sphere shown in C is finally expanded to include one molecule of parent alcohol. The Lewis acidity of $Ce_4O(OR)_{13}$ is thus established, and the frequent occurrence of coordinated alcohol[9] is further extended. Since $Ce_4O(O^iPr)_{13}(^iPrOH)$ contains one Ce^{III} and three Ce^{IV} ions, this formal analysis of the parentage of the Ce_4O core in terms of $Ce^{IV}{}_3O$ (cf. $Ce_3O(O^tBu)_{10}$) and Ce^{III} constituents may have some relevance to its mechanism of formation.

Origin of the Reduction. Sheldon and Kochi[5] established that the photochemical reduction of Ce(IV) (as their carboxylates) involved the intermediacy of alkyl radicals (from decarboxylation of carboxyl radicals). Photochemical homolysis of the $Ce-O_2CR$ bond was suggested. The necessity of primary or secondary alkoxy groups in the synthesis of $Ce_4O(OR)_{13}(ROH)$ suggests that hydrogen transfer from a geminate alkoxy radical also participates here. The resulting cerium(IV) hydride presumably then forms H_2 and Ce(III).

Seeking the Source of the Oxo Ligand. To establish whether isopropoxide is the source of the μ_4-O atom, we have examined the volatile reaction products. After irradiation of $Ce_2(O^iPr)_8(^iPrOH)_2$ in C_6D_6, the volatiles were quantitatively vacuum-transferred (-196 °C) to an NMR tube and analyzed by ^1H NMR spectroscopy. This showed ^iPrOH and acetone (the source of the reducing equivalents) but neither resonance of propane and no signals in the vinyl region (e.g., propylene). In another instance of oxo formation we have detected significant amounts of propane by this procedure.[25]

Acknowledgment. This work was supported by DOE Grant DE-FG02-88ER13906. We thank Scott Horn for skilled technical assistance.

Supplementary Material Available: Listings of full crystallographic details and anisotropic thermal parameters (2 pages); a table of observed and calculated structure factors (9 pages). Ordering information is given on any current masthead page.

(24) Cotton, F. A.; Marler, D. O.; Schwotzer, W. *Inorg. Chim. Acta* **1984**, *95*, 207.

(25) Vaartstra, B. A.; Streib, W. E.; Caulton, K. G. *J. Am. Chem. Soc.* **1990**, *112*, 8593.

Contribution from the Department of Chemistry
Texas A&M University, College Station, Texas 77843-3255

Utility of Semilocalized Bonding Schemes in Extended Systems: Three-Center Metal-Metal Bonding in MoS_2, $H_x(Nb,Ta)S_2$, and ZrS

Kyeong Ae Yee and Timothy Hughbanks*

Received October 9, 1990

A semilocalized description of bonding in extended metal-metal-bonded systems is described for the prototype title compounds. Beginning with calculated band orbitals, we explicitly construct three-center bond orbitals (Wannier functions) for the trigonal-prismatic layer compound MoS_2. While no well-localized single-center functions or two-center bonds can be constructed, the three-center Wannier functions prove to be highly localized. The isoelectronic $LiNbO_2$ can be treated similarly. This provides a very economical description of the M-M bonding in these layer compounds and is shown to be the most natural way of understanding the metal-hydrogen and residual metal-metal bonding in the tantalum and niobium hydrogen bronzes $H_x(Ta,Nb)S_2$. ZrS adopts a WC structure that may be viewed as a 3-D condensation of the 2-D trigonal-prismatic layers present in the aforementioned materials. The 2-D metal-metal bonding description in the layers persists in ZrS as well, in agreement with earlier work by Nguyen and co-workers.

Introduction

In the description of the electronic structure of solids and surfaces there is a widely recognized tension between localized and delocalized bonding viewpoints. In the vernacular of the field it comes down to a dilemma that pits the traditional physicists' delocalized *bands* against the chemists' *bonds*. This situation is familiar to chemists in the contrast between valence bond and molecular orbital theories. While these two approaches differ in several respects, perhaps the most important conceptual difference between the theories lies in the localized nature of the valence bond approach and the delocalization of molecular orbitals. In the intermediate regime are semilocalized descriptions of bonding wherein the multicenter bonding schemes provide chemists a means of "counting electrons" and assigning electron pairs to some combination of two-center-two-electron (Lewis) bonds and, e.g., three-center-two-electron (3c-2e)[1] or three-center-four-electron (3c-4e) systems.[2,3]

The need for chemically useful yet physically realistic localized bonding schemes for solids continues to press. In the present paper, we present some results of our efforts to understand the electronic structures of manifestly extended systems, especially those involving metal-metal bonds. We extract localized orbitals from delocalized band orbitals, using well-known Wannier functions[4-7]

* To whom correspondence is to be addressed.

(1) Lipscomb, W. N. *Boron Hydrides*; Benjamin: New York, 1963.
(2) Pimentel, G. C. *J. Chem. Phys.* **1951**, *19*, 446.
(3) Rundle, R. E. *J. Am. Chem. Soc.* **1963**, *85*, 112.
(4) Wannier, G. H. *Phys. Rev.* **1937**, *52*, 191.

0020-1669/91/1330-2321$02.50/0

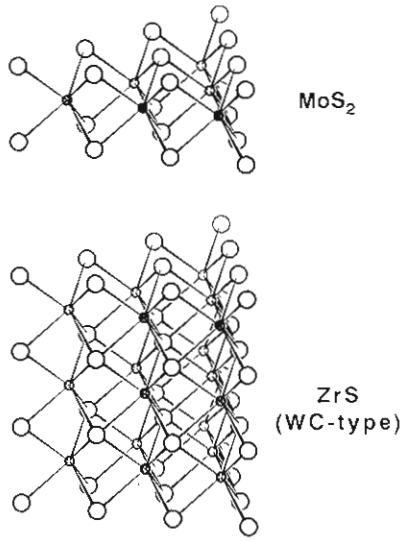

Figure 1. One layer of the MoS_2 structure and the 3-dimensional "condensed MoS_2" WC-type structure of ZrS.

in a context that highlights their potential chemical usefulness and versatility. In order to appraise our methods and because of their intrinsic interest, we have examined several materials in which MX_2 trigonal-prismatic two-dimensional layers can be structurally identified or inferred.[8,9]

We shall concentrate upon layer compounds with trigonal-prismatic transition-metal centers[9] as an entry into the study of localized bonding within extended network solids. Typical examples are the trigonal-prismatic layered dichalcogenides (MX_2; where M = Mo, W and X = S, Se). A single layer of molybdenum disulfide,[10] viewed down the three-fold axis, is shown in **1**. As shown at the bottom of the illustration, each Mo atom

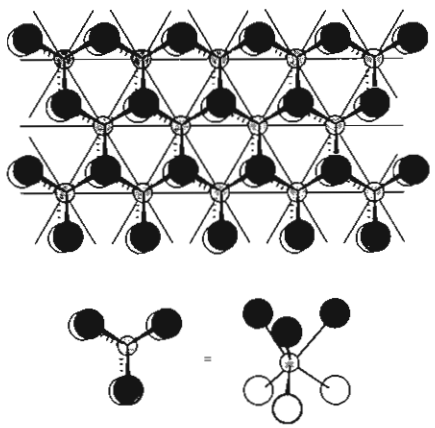

1

is surrounded by a trigonal prism of sulfurs (see the bottom of **1**). The Mo–S bond length is 2.35 Å; each Mo is further surrounded by six Mo centers at 3.16 Å in the plane of the layer. The MoS_6 trigonal prisms may be seen as fused on their rectangular faces with three adjacent prisms. The α- and β-MoS_2 polymorphs (which crystallize in the $R3m$ and $P6_3/mmc$ space groups, respectively) are simply stacking variants built up from these 2-D layers with van der Waals gaps separating the layers. Niobium centers are trigonal prismatic in $LiNbO_2$, which is simply built of NbO_2^- layers with Li^+ ions intercalated.[11,12]

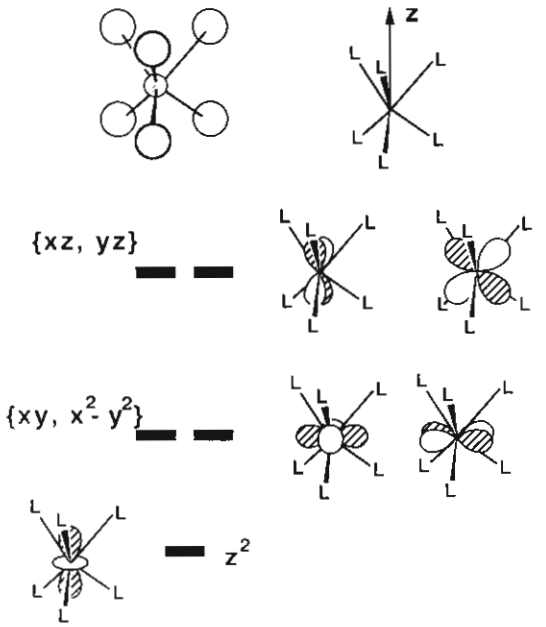

Figure 2. 4d orbital ligand field splitting for Mo in a trigonal-prismatic environment.

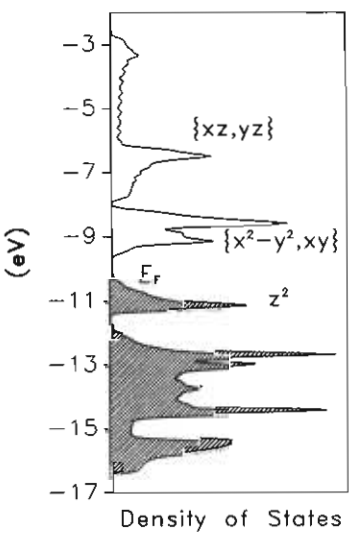

Figure 3. Density of states (DOS) calculated for MoS_2. The occupied levels are shaded. Labels on the bands refer to the conventional labeling in most of the literature and are in correspondence with the labeling in Figure 2.

The three-dimensional material ZrS adopts an tungsten carbide structure.[13] This simple structure, consisting of interpenetrating simple hexagonal arrays of metals and nonmetals, may also be viewed as a result of the condensation (at sulfur) of the MoS_2 structure (see Figure 1).

We turn first to the trigonal-prismatic layer compound MoS_2 in order to illustrate how localized bonding information can be extracted from the electronic structure calculations. We used the extended Hückel method throughout; parameters and other computational details are given in the Appendix. MoS_2 is known to be a diamagnetic semiconductor, and this is traditionally understood by reference to the ligand field splitting experienced by the Mo 4d orbitals in a trigonal-prismatic environment. As indicated in Figure 2, the z axis is chosen collinear with the 3-fold axis and the splitting pattern shown is easily understood. Since

(5) Ziman, J. M. *Principles of the Theory of Solids*; Cambridge University Press: London, 1964.
(6) Slater, J. C. *Quantum Theory of Molecules and Solids*; McGraw-Hill: New York, 1965.
(7) Kittel, C. *Quantum Theory of Solids*; John Wiley & Sons: New York, 1963.
(8) Wilson, J. A.; Yoffe, A. D. *Adv. Phys.* **1961**, *18*, 193.
(9) Hulliger, F. *Struct. Bonding* **1967**, *4*, 83.
(10) Dickinson, R.; Pauling, L. *J. Am. Chem. Soc.* **1923**, *45*, 1466.
(11) (a) Meyer, G.; Hoppe, R. *Angew. Chem., Int. Ed. Engl.* **1974**, *13*, 744. (b) Meyer, G.; Hoppe, R. *Z. Anorg. Allg. Chem.* **1976**, *424*, 128.
(12) Geselbracht, M. J.; Richardson, T. J.; Stacy, A. M. *Nature* **1990**, *345*, 324.
(13) Nguyen, T.-H.; Franzen, H.; Harmon, B. N. *J. Chem. Phys.* **1980**, *73*, 425.

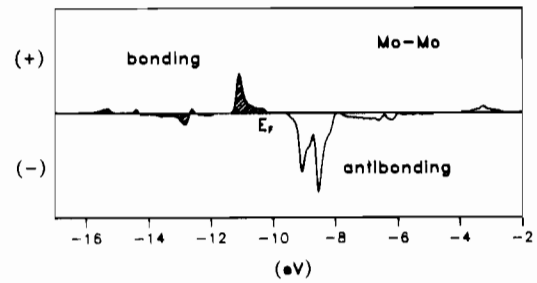

Figure 4. Crystal orbital overlap population (COOP) plot for the Mo–Mo bonds in MoS_2 layer. The energy axis is horizontal and the COOP is vertical and occupied levels shaded. Notice that Mo–Mo bonding levels are optimally occupied.

the sulfur ligands lie in or near the nodal cone of the d_{z^2} orbital, this orbital should be Mo–S nonbonding and will lie lowest. The $\{d_{xz}, d_{yz}\}$ pair is most strongly directed at the surrounding ligands and have the greatest Mo–S σ antibonding character, while the $\{d_{x^2-y^2}, d_{xy}\}$ set will be intermediate in their interaction with sulfur donor orbitals. In the total DOS (density of states) plotted for the condensed system in Figure 3, it appears that the splitting pattern is conserved.[14] Above the sulfur p bands there are three peaks that are conventionally said to correspond to the $d_{z^2} < d_{x^2-y^2}$, $d_{xy} < d_{xz}$, d_{yz} ordering expected from the ligand field splitting diagram and are labeled as such in our figure. However, there are some differences. First of all, we see considerable mixing between the d_{z^2} and the $\{d_{x^2-y^2}, d_{xy}\}$ set in our (and many others') calculations[8,15-19]—the lower d band labeled "z^2" contains 40% of d_{z^2} and 44% of $\{d_{x^2-y^2}, d_{xy}\}$ while most of the remainder is S p in character. Naturally, the band labeled "$x^2 - y^2$, xy" reflects a similar mixing (23.0% d_{z^2} and 55.8% $\{d_{x^2-y^2}, d_{xy}\}$). The gap between these bands (1.2 eV observed, we calculate 0.82 eV) can be explained only when this mixing is acknowledged.[20,21] For the isostructural NbO_2^- layers in $LiNbO_2$, one of us reported calculations showing an even greater mixing of the of orbital character between these bands (31.3% d_{z^2} and 42.8% $\{d_{x^2-y^2}, d_{xy}\}$ in the nominally "z^2" band).[22] We note here that scanning tunneling microscopy (STM) has been applied to the study of MoS_2 and related materials, and some interpretations of the data have centered on assuming that one observes valence electron density in the d_{z^2} orbitals.[23-26] These data offer no firm information relevant to the present paper, in part because of uncertainties as to the interpretation of STM data.

A plot of the Mo–Mo crystal orbital overlap population (COOP) curve for Mo–Mo bonds in MoS_2 shows the Fermi level bisects the Mo–Mo bonding–antibonding divide (Figure 4). It seems that Mo–Mo bonding is an important factor stabilizing the structure. The Mo–Mo contacts are 3.16 Å, and the calculated Mo–Mo overlap population at this distance is 0.054—indicative of a modest bonding interaction between metals, which is not strong, but each Mo interacts with six metal neighbors.

Now let us take our analysis some steps further and ask more specific and probing questions. *Where* are the Mo–Mo bonds in this structure—where do the electrons spend their time? We calculate a larger band gap for $LiNbO_2$ than for MoS_2 even though the shorter Nb–Nb contacts in the former compound might have led us to expect a broader "z^2" and "$x^2 - y^2$, xy" bands and hence a smaller gap between them—why? Is there a simpler, perhaps more *chemical*, way of understanding why d^2 trigonal-prismatic layer compounds are semiconductors, in spite of significant metal-metal interactions and the presence of an extended hexagonal metal–metal-bonded network? How will the insertion of hydrogen into the metal layer in the $H_x(Ta,Nb)S_2$ bronzes perturb the electronic structure and why does MoS_2 not show similar behavior? Are there electronic as well as structural similarities between ZrS and MoS_2? We will endeavor to answer these questions and comment on the broader implications of our treatment.

From Band Orbitals to Bond Orbitals

Transformations between delocalized molecular orbitals and localized bond orbitals or group orbitals are a familiar procedure throughout molecular chemistry.[6,27-30] For the simplest of organic molecules, methane, one may take linear combinations of the four occupied valence molecular orbitals (a_{1g} and t_{1u}) to construct four equivalent C–H bond orbitals that span the same irreducible representations. It is also well-known that the total Hartree–Fock single determinant wave function is unaffected by such a unitary transformation.[6] By similar procedures one may, for example, interrelate the molecular orbital description of the bonding of bridging hydrides in B_2H_6 to the semilocalized bonding description of diborane where two three-center B–H–B bonds are identified. Kettle pointed out that 12 edge-bonding localized orbitals for the $M_6X_8^q$ clusters (for example, with M = Mo, X = Cl, and q = 4+[31-33] or with M = Re, X = S, and q = 2+)[34-38] span the same irreducible representations in the O_h point group as the 12 bonding MOs discussed above in our treatment of M_6X_8 clusters. One may therefore construct a set of such localized bond orbitals from combinations of the delocalized orbitals and vice-versa.[30] The eight occupied Ta MOs of the $Ta_6Cl_{12}^{2+}$ cluster[39,40] transform the same as eight face-bonding (3c–2e) localized orbitals, and therefore a semilocalized scheme can be constructed for this cluster as well.[30] In the following section, we subject the metal-metal bonding in MoS_2 to an analogous analysis.

We first summarize the formal procedures we have followed. In dealing with electronic wave functions for solids, localized orbitals are constructed by forming Wannier functions.[4-6,41-43] These are constructed from the crystal orbitals (the one-electron wave functions), and the crystal orbitals are in turn built up from symmetrized (Bloch) basis orbitals ($\chi_{i,\mathbf{k}}$)

$$\chi_{i,\mathbf{k}} = \frac{1}{N^{1/2}} \sum_{\mathbf{R}} e^{i\mathbf{k}\cdot\mathbf{R}} \chi_i(\mathbf{r} - \mathbf{R}) \qquad (1)$$

where i is a label that runs over the list of atomic orbitals in a unit cell, $\mathbf{R}$ is a lattice vector that specifies the displacement of a unit cell from the origin cell, and N is the number of unit cells

(14) For references to the numerous electronic structure calculations on MoS_2 and other layer compounds, see: Doni, E.; Girlanda, R. In *Electronic Structure and Electronic Transitions in Layered Materials*; Grasso, V., Eds.; D. Reidel: Dordrecht, Holland; 1986.
(15) Mattheiss, L. F. *Phys. Rev. Lett.* **1973**, *30*, 784.
(16) Mattheiss, L. F. *Phys. Rev. B* **1973**, *8*, 3719.
(17) Bromley, R. A. *Phys. Rev. Lett.* **1972**, *29*, 357.
(18) Bromley, R. A.; Murray, R. B.; Yoffe, A. D. *J. Phys. C* **1972**, *5*, 746.
(19) Huisman, R.; Dejonge, R.; Haas, C.; Jellinek, F. *J. Solid State Chem.* **1971**, *3*, 56.
(20) Beal, A. R.; Liang, W. Y.; Hughes, H. P. *J. Phys. C* **1976**, *9*, 2449.
(21) Amirtharaj, P. M.; Pollak, F. M.; Wold, A. *Solid State Commun.* **1982**, *41*, 581.
(22) Burdett, J. K.; Hughbanks, T. R. *Inorg. Chem.* **1985**, *24*, 1741.
(23) Tang, S. L.; Kasowski, R. V.; Parkinson, B. A. *Phys. Rev. B* **1989**, *39*, 9987.
(24) Weimer, M.; Kramer, J.; Bai, C.; Baldeschwieler, J. D. *Phys. Rev. B* **1988**, *37*, 4292.
(25) Stupian, G. W.; Leung, M. S. *Appl. Phys. Lett.* **1987**, *51*, 1560.
(26) Sarid, D.; Henson, T. D.; Armstrong, N. R.; Bell, L. S. *Appl. Phys. Lett.* **1988**, *52*, 2252.
(27) Albright, T. A.; Burdett, J. K.; Whangbo, M.-H. *Orbital Interactions in Chemistry*; John Wiley & Sons: New York, 1985.
(28) Edmiston, C.; Ruedenberg, K. *Rev. Mod. Phys.* **1963**, *35*, 457.
(29) Jorgensen, W. L.; Salem, L. *The Organic Chemist's Book of Orbitals*; Academic Press: New York, 1973.
(30) Kettle, S. F. A. *Theor. Chim. Acta* **1965**, *3*, 211.
(31) Brosset, C. *Ark. Kemi* **1949**, *1*, 353.
(32) Brosset, C. *Ark. Kemi, Mineral. Geol.* **1945**, *A20*, 16.
(33) Brosset, C. *Ark. Kemi, Mineral. Geol.* **1946**, *A22*, 10.
(34) Bronger, W.; Miessen, J.-J. *J. Less Common Met.* **1980**, *76*, 73.
(35) Bronger, W.; Miessen, J.-J. *J. Less Common Met.* **1982**, *83*, 29.
(36) Bronger, W.; Miessen, J.-J.; Neugroschel, R. *J. Less Common Met.* **1985**, *105*, 303.
(37) Perrin, A. *New J Chem.* **1990**, *14*, 561–567.
(38) Spangenberg, M.; Bronger, W. *Angew. Chem., Int. Ed. Engl.* **1978**, *17*, 368.
(39) Vaughan, P. A. *Proc. Nat. Acad. Sci. U.S.A.* **1950**, *36*, 461.
(40) Vaughan, P. A.; Sturtivant, J. H.; Pauling, L. *J. Am. Chem. Soc.* **1950**, *72*, 5477.
(41) Monkhorst, H. J.; Kertesz, M. *Phys. Rev. B: Condens. Matter* **1981**, *24*, 3015.
(42) Coizeaux, J. d. *Phys. Rev.* **1964**, *135*, A698.
(43) Cloizeaux, J. d. *Phys. Rev.* **1964**, *135*, A685.

in the crystal. The wave vector **k** runs over the N allowed values within the first Brillouin zone, as discussed in standard solid-state physics texts.[44,45] The crystal oribtals, $\phi_{\mathbf{k},n}$, are obtained as linear combinations of these Bloch basis orbitals:

$$\phi_{\mathbf{k},n} = \sum_i c_{i,n}(\mathbf{k})\chi_{i,\mathbf{k}} \tag{2}$$

where n is the band index—a label for the bands running from the lowest in energy to the highest. A Wannier function for each band can be built up around the lattice site **R** by employing the following prescription:

$$\omega_n(\mathbf{r} - \mathbf{R}) = \frac{1}{N^{1/2}}\sum_{\mathbf{k}}^{\mathrm{BZ}} e^{-i\mathbf{k}\cdot\mathbf{R}}\alpha_{\mathbf{k}}\phi_{\mathbf{k},n} \tag{3}$$

In this expression, we have explicitly included the phase factor $\alpha_{\mathbf{k}}$ as a reminder that any orbital wave function $\phi_{\mathbf{k},n}$ is uncertain to within an arbitrary phase factor. It is a property of Wannier functions that for each lattice site **R** the Wannier function $\omega_n(\mathbf{r} - \mathbf{R})$ is identical with the function centered in the origin unit cell, modulo a translation by the vector **R**. So it is simpler to restrict our attention to the Wannier function centered in the origin cell ($\omega_n(\mathbf{r})$)

$$\omega_n(\mathbf{r}) = \frac{1}{N^{1/2}}\sum_{\mathbf{k}}^{\mathrm{BZ}} \alpha_{\mathbf{k}}\phi_{\mathbf{k},n} \tag{4}$$

Just how well localized Wannier functions can be depends upon the nature of the band orbitals *and* upon our choice of the arbitrary phases $\alpha_{\mathbf{k}}$. For example, if crystal orbitals $\phi_{\mathbf{k},n}$ are built up from just *one* Bloch basis orbital, then in constructing the Wannier functions $\omega_n(\mathbf{r} - \mathbf{R})$, we get out nothing more than the original, localized, atomic orbitals.

The arbitrariness in Wannier functions due to our freedom to vary the phases $\alpha_{\mathbf{k}}$ does not influence the fact that *as a set* the functions $\{\omega_n(\mathbf{r} - \mathbf{R}),$ all $\mathbf{R}\}$ give the same electron density for the nth band as the set of crystal orbitals $\{\phi_{\mathbf{k},n},$ all $\mathbf{k}\}$. We can just as validly discuss the bonding for the nth band using either set of orbitals, as suits our purposes. In particular, if the directional nature of the band orbitals is obscured because there are so many to consider and that they are manifestly delocalized over the entire crystal, then appropriately constructed localized orbitals may immensely clarify matters.

Three-Center Bonds in Trigonal-Prismatic Layers

With the preceding ideas in mind, we turn our attention to the "z^2" band of MoS_2. We wished to see whether a description of the Mo–Mo bonding in these layers involving 3c–2e bonds is appropriate. One reason for believing this might be the case is that there is one Mo_3 triangle uncapped by sulfur per metal center in the layer (each center is shared by three such triangles). This means that we do not lose the electron-counting scheme that rationalizes the semiconducting behavior of the material, it is just that instead of assigning two electrons to each d_{z^2} orbital, they are understood to reside in a three-center bonding orbital. To construct localized bond orbitals we first placed a "probe" hydrogen 1s orbital in the center of a given Mo_3 triangle. The hydrogen isn't included in the band structure calculation, but this doesn't prevent us from calculating the overlap of $\phi_{\mathbf{k},n}$ with our probe orbital. As the functions $\phi_{\mathbf{k},n}$ emerge from our calculations, they have essentially arbitrary phase so this overlap is expressed as a complex number; $\langle 1s|\phi_{\mathbf{k},n}\rangle = |S|\exp(i\theta)$. Then for the phase factor we choose $\alpha_{\mathbf{k}} = \exp(-i\theta)$ so that the phase shifted orbital $(\alpha_{\mathbf{k}}\phi_{\mathbf{k},n})$ has a real, positive overlap with the probe orbital. Additional details are discussed in the Appendix. For the localized Wannier orbital, our procedure has the effect of maximizing its amplitude in the Mo_3 triangle where the probe orbital was placed.

The bond orbital obtained by this procedure is the symmetrical and very well-localized function for which orbital contours are plotted in the layer plane in Figure 5. Only a small contribution

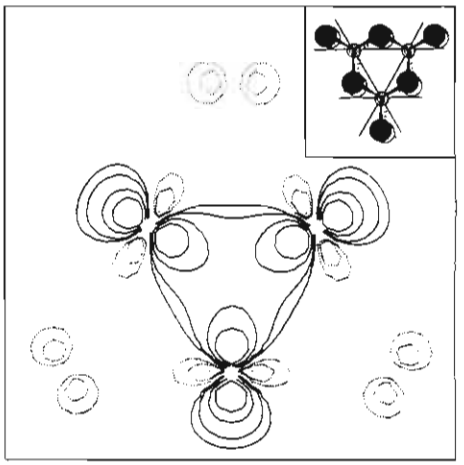

Figure 5. Contour plots for the localized 3c–2e bonding orbital in the layer plane. The contours are ±0.3, ±0.17, ±0.10, and ±0.04.

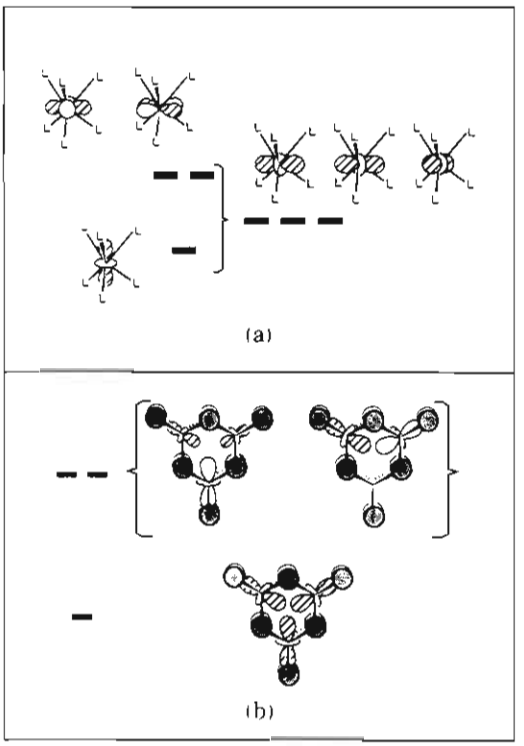

Figure 6. (a) Three identical orthogonal orbitals that are constructed from d_{z^2}, $\{d_{x^2-y^2}, d_{xy}\}$ orbitals. (b) Three-center bond orbitals built from in-plane d orbitals in part a.

from three Mo centers adjacent to the triangle can be discerned and a limited contribution from the sulfur centers comes in as well (as it must—remember that these functions must exactly reflect the electron density present in the band orbitals from which they were constructed). Identical orbitals may be constructed in each of the uncapped Mo_3 triangles in the layer, and the system has two electrons to place in each.

In retrospect, we can understand the results obtained by returning to the orbitals of the imbedded trigonal-prismatic Mo centers shown in Figure 2. If we construct combinations from the three lowest lying d orbitals, d_{z^2} and $\{d_{x^2-y^2}, d_{xy}\}$, we can obtain three identical, orthogonal orbitals (σ_1, σ_2, σ_3—see eq 5) that

$$\begin{aligned}
\sigma_1 &= \frac{-1}{3^{1/2}}d_{z^2} + \left(\frac{2}{3}\right)^{1/2} d_{x^2-y^2} \\
\sigma_2 &= \frac{-1}{3^{1/2}}d_{z^2} - \frac{1}{6^{1/2}}d_{x^2-y^2} - \frac{1}{2^{1/2}}d_{xy} \\
\sigma_3 &= \frac{-1}{3^{1/2}}d_{z^2} - \frac{1}{6^{1/2}}d_{x^2-y^2} + \frac{1}{2^{1/2}}d_{xy}
\end{aligned} \tag{5}$$

(44) Harrison, W. A. *Solid State Theory*; Dover: New York, 1980.
(45) Ashcroft, N. W.; Mermin, N. D. *Solid State Physics*; Holt, Rinehart and Winston: New York, 1976.

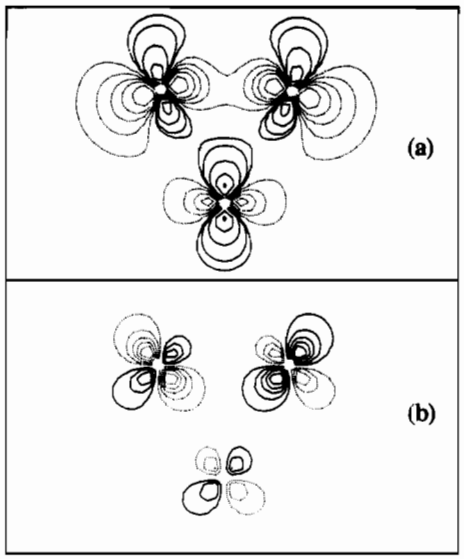

Figure 7. Contour plots for two members of the e′ set. Contours are ±0.4, ±0.3, ±0.2, and ±0.1.

extend primarily in the *xy* plane as we illustrate in Figure 6a. If we start with these orbitals, the three-center bond orbitals can be constructed as shown in Figure 6b. As this figure implies, we should be able to find not only the totally symmetric (a_1') orbital but the antibonding e′ set as well. We constructed a localized set of orbitals from the "$x^2 - y^2$, xy" bands, only this time p_x and p_y orbitals placed in the triangle centers served as the probes to determine the α_k phase factors. The resultant local orbitals shown in Figure 7 do indeed resemble the idealized e′ set indicated in Figure 6b.

Our orbital plots (Figures 5 and 7) do mask the fact that there is still as much d_{z^2} character in the valence band as d_{xy}, $d_{x^2-y^2}$ character. Thus, for this sytem the ideal mixing coefficients of these two sets (as shown in eq 5), are not quite achieved and a plot of the localized a_1' orbital in a plane orthogonal to the layer plane and through a line containing the triangle center and a Mo center shows the a_1' orbital has considerable d_{z^2} character. We have constructed similar plots for the NbO_2^- layer in $LiNbO_2$, where the smaller oxides allow the metal–metal separation to shrink to 2.90 Å. As stated earlier, we obtain even more d_{xy}, $d_{x^2-y^2}$ mixing and the three-center bonding picture is even more appropriate. Since the valence-conduction band splitting in this picture is due to the splitting between the a_1' and e′ localized orbitals, the larger calculated splitting compared to MoS_2 is easily understood as arising from stronger metal–metal interaction.

We should note that the construction of local (Wannier) orbitals does involve a seeming arbitrariness that is expressed, mathematically, through our freedom to vary the α_k phase factors. Thus, we might have attempted to construct local orbitals for the valence band in MoS_2 that would give us a picture that more closely conforms to the conventional picture of this band as a "z^2" band. This is a straightforward thing to do: we just choose the α_k coefficients so that the d_{z^2} orbital coefficient in each crystal orbital ($\alpha_k \phi_{k,n}$) for the metal center in question is real and positive. To the greatest extent possible, the resulting orbital will be localized as a d_{z^2} orbital on the metal center in question. For MoS_2, when this is done, the resulting orbital is *not* well localized but has a significant spread over the six neighboring metal centers and beyond. It is not difficult to recognize this rather poorly localized orbital as a symmetric linear combination of three adjacent three-center bond orbitals such as plotted in Figure 5. The reason for the poorer localization in this case can be understood on symmetry grounds. A local orbital built up as described must be symmetric with respect to the 3-fold axis that goes through the central metal and so the local orbital can have no $\{d_{x^2-y^2}, d_{xy}\}$ character at the central metal. But since the valence band *does* have considerable $\{d_{x^2-y^2}, d_{xy}\}$ character, this must be found on the neighboring metals. In a similar test of our ideas concerning local orbitals for this system, we found that an attempt to localize an orbital within the triangles that are capped by sulfur also fails. In this case, we were simply trying to localize the orbital into a location where the valence band charge density is very low—no mathematical manipulation can change this result!

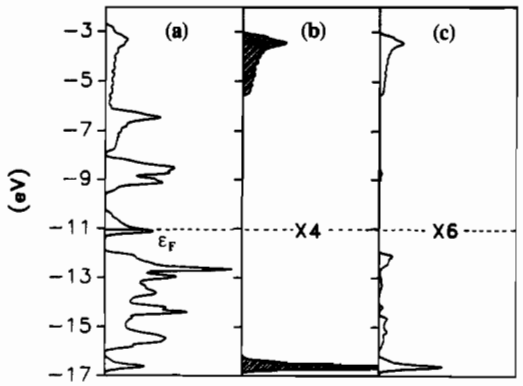

Figure 8. (a) Total DOS plot for $H_{0.33}MS_2$. The Fermi level is appropriate for M = Nb or Ta. (b) DOS contributions for two bands present in the $H_{0.33}MS_2$ system that are not present in the MS_2 system. The lower band has M_3H bonding character; the upper band has M_3H antibonding character. (c) Projected hydrogen contribution to the DOS.

Three-Center Bonds in $H_x(Ta,Nb)S_2$

Murphy and co-workers showed that the trigonal prismatic TaS_2 and NbS_2 (the so-called 2H– polytypes) can be cathodically reduced to form $H_x(Ta,Nb)S_2$:[46]

$$xH^+ + (Nb,Ta)S_2 + xe^- \rightarrow H_x(Nb,Ta)S_2 \quad 0 < x < 0.87$$

Neutron powder diffraction data and NMR evidence showed that hydrogen is located in the triangular interstices, within the metal layers.[47,48] The mean Ta–Ta distance in $H_{0.66}TaS_2$ is 3.34 Å (which is just the lattice parameter, *a*, since no deuterium long-range ordering was detected in the neutron diffraction study). This value is little changed from 3.32 Å for TaS_2 itself. If the Ta centers continue to form an undistorted hexagonal array, then the Ta–H distance is 1.93 Å, which is not an unreasonable value when compared with M–H distances for various bridging modes in polynuclear hydride clusters.[49]

The previous discussion carries obvious implications for the binding of hydrogen in the triangular interstices of the $H_x(Ta,Nb)S_2$ bronzes. A hydrogen interstitial, with a half-filled totally symmetric 1s orbital, should interact strongly with only the *half*-occupied (in TaS_2 or NbS_2) three-center bonding band. On the other hand, in the MoS_2 system, an electron would be forced into the antibonding conduction band. This has been assumed in the past,[50] but without the kind of analysis we have presented, this conclusion is far from obvious. If one neglects the mixing between the d_{z^2} and $\{d_{x^2-y^2}, d_{xy}\}$ orbitals in the valence and conduction bands, then it might be expected that the conduction band orbitals (that ostensibly have "$x^2 - y^2$, xy" character) should overlap best with the interstitial hydrogen and behave as acceptor orbitals for a hydride donor. We discuss the details of the hydrogen–MS_2 interaction below.

We calculated the band structure for a hypothetical ordered $H_{0.33}MS_2$ layer (M was given Mo parameters, but Nb parameters would yield essentially the same results). In the calculation, hydrogens were simply placed in every third M_3 interstice so that the system remains hexagonal with an supercell lattice parameter $a' = \sqrt{3}a$. The resultant DOS plot is shown in Figure 8. Comparison of Figure 3 and the total DOS plot in Figure 8a indicates that the band structure is remarkably unaltered by

(46) Murphy, D.; Hull, G. W. J. *J. Chem. Phys.* **1975**, *62*, 967.
(47) Riekel, C.; Reznik, H. G.; Schöllhorn, R.; Wright, C. J. *J. Chem. Phys.* **1979**, *70*, 5203.
(48) Kleinberg, R. L.; Jacobson, A. J.; Silbernagel, B. G.; Halbert, T. R. *Mater. Res. Bull.* **1980**, *15*, 1541.
(49) Anderson, A. B.; Al-Seigh, Z. Y.; Hall, W. K. *J. Phys. Chem.* **1988**, *92*, 803.
(50) van Santen, R. A. *J. Mol. Struct.* **1988**, *173*, 157.

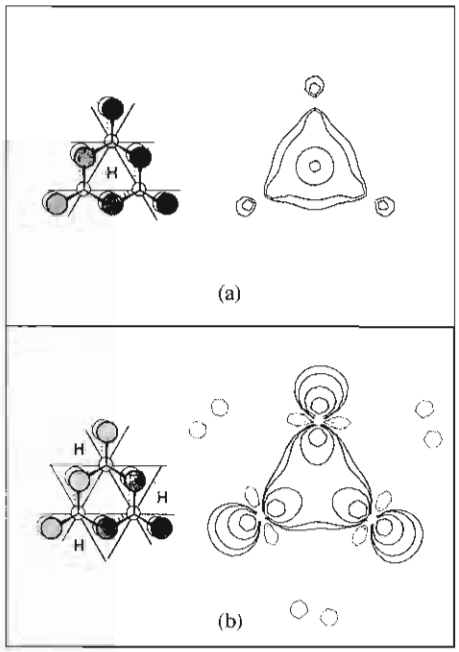

Figure 9. (a) Localized orbital built from the hydridic M_3H bonding band. Contours are ±0.25, ±0.12, ±0.06, and ±0.04. (b) Localized bonding orbitals from the valence band on the "unprotonated" M_3 triangle sites. Note the close match with Figure 5. Contours are ±0.3, ±0.17, ±0.10, and ±0.04.

inclusion of hydrogen except for features that are highlighted in the two additional panels. In Figure 8b, we show the density of states attributable to two particular bands. The lower band is apparent in total DOS plot just beneath the sulfur p block. The upper band in this panel lies at an energy such that it is obscured by the *xz*, *yz* bands, but this energy overlap should not be interpreted as indicating some mixing between the orbitals for this band and the metal $\{d_{xz}, d_{yz}\}$ orbitals. Indeed, both of the bands highlighted in the center panel involve orbitals that are symmetric with respect to the plane containing the metals, and the antisymmetric $\{d_{xz}, d_{yz}\}$ orbitals make no contribution. An alternative interpretation of Figure 8b is that it represents the DOS difference between the the $H_{0.33}MS_2$ and MS_2 systems in the energy ranges −17.0 to −16.0 eV and −6.0 to −3.0 eV. The only other region of the DOS that shows a significant change is the three-center bonding valence band, where the band shape and spread in energy change very little, but the area (number of levels) decreases by one-third. The hydrogen contribution to the DOS projected in Figure 8c is greatest within the two bands depicted in Figure 8b, although modest mixing of the hydrogen 1s orbital into the formal sulfur p block can also be seen. The hydrogen 1s orbital contributions are conspicuous by their absence in both the valence band ("z^2") and conduction band ("$x^2 - y^2$, xy").

The use of localized orbitals makes the interpretation of the metal–hydrogen interaction transparent. Displayed in Figure 9 are two local orbitals, in Figure 9a the local orbital is constructed from the lower band of Figure 8b, in Figure 9b a local orbital for the valence band is shown. Since the former band has considerable hydridic character, the only well-localized orbitals that can be constructed are those which are symmetric about the hydrogen centers. This lower band is easily understood as resulting from a bonding interaction of the hydrogen 1s orbital with the M_3 three-center bonding orbital we have discussed earlier. The antibonding counterpart to this band is just the upper band as shown in Figure 8b and for the sake of brevity, the corresponding local orbital is not shown. As noted above, the valence band has a negligible hydrogen s orbital contribution and it has a form that is remarkably unchanged from MoS_2, as seen by comparison with Figure 3 (except, of course, that the valence band is fully occupied in MoS_2 and partially occupied in $H_x(Nb,Ta)S_2$). Because there is no hydrogen character in this band, it is not possible to construct a well-localized orbital in the hydrogen-filled triangles. On the contrary, if we simply localize the valence band orbitals in the unfilled triangles, we find the local orbitals to be virtually identical with the corresponding local orbitals for the unhydrogenated material. Thus, the electronic effect of hydrogen inclusion can be understood in a very simple manner within the localized framework: The hydrogen 1s orbital interacts significantly only with the three-center bonding orbitals for the triangles in which they sit. This interaction gives rise to bonding and antibonding combinations that form the basis for the two bands singled out in Figure 8b.

The above conclusions are underscored by pointing out which orbitals do *not* interact with the included hydrogen. The band which we have identified with e′ orbitals of the M_3 three-center systems (the conduction band of MoS_2) do not significantly interact with the hydrogen interstitial because, as seen in Figure 7, each local orbital has a node through the hydrogen. Furthermore, for $H_{0.33}MS_2$ the valence band local orbitals that are symmetric with respect to the center of the *unprotonated* triangles naturally have little interaction with the H 1s orbitals in the *protonated* triangles. Thus, the only noticeable change in the valence band peak is that its area decreases by one-third, simply because one-third of the localized three-center bonding orbitals are involved in the M_3H bonding and antibonding bands we discussed above.

In the local framework, the analysis we have discussed is straightforward. Our conclusions regarding the hydrogen–MS_2 interaction would be far less obvious if we proceeded on the basis of the conventional picture of the electronic structure of trigonal-prismatic layered materials. In that picture, one would expect that the "$x^2 - y^2$, xy" conduction band would interact to the *greatest* extent with the hydrogen interstitial because it is seen as built up from the in-plane d orbitals. Our analysis shows that the opposite holds; the so-called "$x^2 - y^2$, xy" band has a negligible interaction with the hydrogen, and it is the three-center bonding orbitals (formerly labeled as "z^2") that have the only appreciable overlap with the interstitial hydrogen 1s orbital. In MoS_2 these levels are filled and in the group V compounds they are only half-filled, so it is with the latter materials that the metal–hydrogen atom interaction is most stabilizing. In MoS_2, each hydrogen bound within the metal layers would require one electron to be pushed into the higher lying conduction band (with Mo–Mo antibonding character—see Figure 7).

ZrS

The above results suggest that in a limited sense, trigonal-prismatic layer compounds are just condensed trinuclear clusters! We decided to take this logic a step further and see whether the trigonal-prismatic layers imbedded in the WC-type ZrS have any electronic "memory" of the condensation from trigonal-prismatic layers we discussed earlier in reference to Figure 1. Part of our motivation stemmed from a statement made by Nguyen and co-workers that the electron density profiles calculated for this material using an APW method suggested 3c–2e bonds in the trigonal-prismatic layers of this material.[13]

Our calculated DOS is shown in Figure 10, and COOP curves for the in-plane and out-of-plane Zr–Zr "bonds" are illustrated in Figure 11. (The DOS and dispersion curves for the high-symmetry lines in the hexagonal Brillouin zone show close similarity with the calculations of Nguyen and co-workers; the latter plots are available as supplementary material.) The DOS shows a deep minimum at the Fermi level (at the d^2 level) that is the result of the splitting off of a single occupied band from the remainder of the Zr d block. Inspection of the COOP curves show that this band does indeed have Zr–Zr bonding character, but it is only appreciable for the Zr–Zr bonds *in* the trigonal-prismatic layers. This is true despite the fact that the interlayer and intralayer Zr–Zr distances are nearly equal (3.454 and 3.430 Å, respectively).

Finally, we have also included the projection of the symmetric three-center bond orbital as the shaded portion of the DOS in Figure 10. Because the linear combination of atomic orbitals that make up the three-center bond orbital are determined by overlap

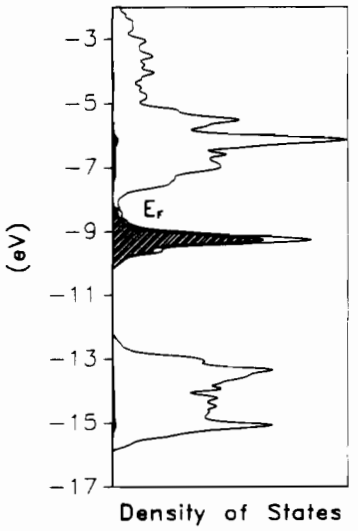

Figure 10. Total DOS plot for ZrS. The shaded area corresponds to the projection of the three-center bonding orbital combination. By noting the position of the Fermi level, it can be seen that the filled region of the d band corresponds to the filling of three-center Zr–Zr bonding orbitals.

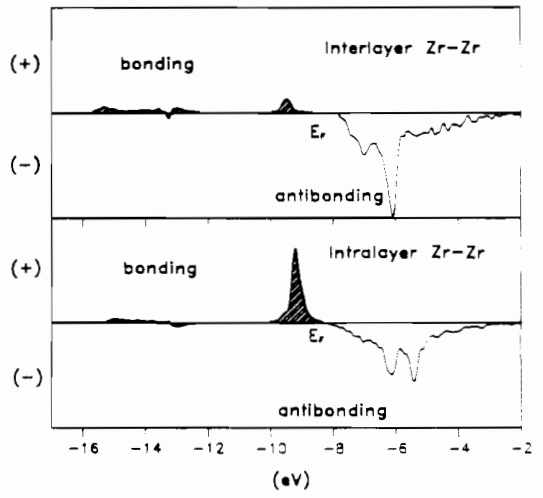

Figure 11. COOP curves for the intralayer (bottom) and interplane (top) Zr–Zr bonds. All shaded areas are occupied. The comparison indicates an appreciable bonding interaction only between metals within the MoS_2-like layers.

with a "probe" hydrogen as described earlier, this projected DOS is quite analogous to the procedure described by van Santen for constructing "metal surface group orbitals" that are useful in the analysis surface–adsorbate interactions.[51] This indicates that attempts to construct localized three-center Zr_3 bond orbitals for this band should yield orbitals quite similar to that for MoS_2, and this is precisely what we obtain. Our local orbital contour plots for the occupied d band levels is quite similar to that shown for MoS_2 in figure 5. Thus, this important characteristic of the "clusters within trigonal prismatic MS_2 layers" survives even in this fully condensed system.

Conclusions

One of the most poorly kept secrets of chemical bonding theorists is the fact that electronic structure calculations are relatively easily performed (especially when one is doing approximate calculations and the computer codes are written)! The difficult part comes when we are asked to extract some meaning from the computed results and to provide conclusions beyond those which our programs are explicitly designed to produce. This proves to be especially true of band structure calculations and our ideas of bonding in solids. It seems unlikely that the nature of the chemical bond in molecules and solids is very different, it is just that we need to expend more effort in finding the similarities.

In the present paper, we have shown that, even in some systems with unbroken, extended metal–metal-bonded networks, we can find the molecule-like aspects of the metal–metal bonding. Important to us is the added example of the niobium and tantalum hydrogen sulfide bronzes in which we have a simple prototypical "interstitial" compound and the metal–interstitial bonding is understood from a very chemical, local viewpoint. In all cases, our treatment is completely compatible with the delocalized picture as well since we construct the local orbitals from the delocalized wave functions.

Table I. Parameters for EH calculations

atom	orbital	H_{ii}, eV	ζ_1[b]	ζ_2[b]	c_1[a]	c_2[a]
Zr	4d	−8.59	3.84	1.505	0.6213	0.5798
	5s	−8.48	1.82			
	5p	−4.86	1.78			
Nb	4d	−12.10	4.08	1.64	0.6401	0.5516
	5s	−10.10	1.89			
	5p	−6.86	1.85			
Mo	4d	−11.06	4.54	1.90	0.5899	0.5899
	5s	−8.77	1.96			
	5p	−5.60	1.90			
O	2s	−32.3	2.275			
	2p	−14.8	2.275			
S	3s	−20.0	2.12			
	3p	−13.3	1.83			

[a] Coefficients used in double-ζ expansion. [b] Slater-type orbital exponents.

Acknowledgment. Partial support of this research was derived from a grant (No. 010366-111) by the Texas Advanced Research Program. We also acknowledge the National Science Foundation for its support through a Presidential Young Investigator Award (Grant DMR-8858151) and the Robert A. Welch Foundation for its support through Grant A-1132. Mr. Mike Green is thanked for his work in the early stages of our work on orbital localization.

Appendix

The extended Hückel method was used for all band structure calculations; parameters appear in Table I. Valence state ionization energies (H_{ii}'s) for Zr were obtained from a charge iterative calculation on ZrS. Other parameters have been cited previously.[22,52,53] Structural parameters for $LiNbO_2$, MoS_2, and ZrS were taken from crystallographic data, subject to the simplifications discussed in the text.

Band structure calculations were carried out by using k-point meshes as follows: MoS_2, 91 k points (two dimensional hexagonal lattice); $H_{0.33}MS_2$, 91 k points for the 10 atom hexagonal cell; ZrS, 252 k points for the three dimensional hexagonal cell. Each of these k-point meshes refer to the number of points used in the irreducible wedge of the appropriate Brillouin zones. All DOS curves were smoothed with Gaussian functions with a standard half-width of 0.05 eV.

Wannier functions were constructed by following the general prescription outlined in eq 3 and 4. In all cases, one must include enough k points (N_k) in the entire first Brillouin zone for the band structure calculations so that the extent of localization of the Wannier functions is unaffected by the inclusion of more k points. In practice this means that the Wannier function must be well localized within a radius, r_0, such that

$$r_0 \approx \frac{(N_k)^{1/n}}{2} a$$

where a is a typical lattice parameter for the system and n is the dimensionality of the system (n = 1, 2, 3). For the calculation of Wannier functions for MoS_2, we found it convenient to triple the size of the two-dimensional unit cell so that entire Mo_3 triangle was contained within it. With this expanded cell, we performed

(51) Basch, H.; Gray, H. B. *Theor. Chim. Acta* **1966**, *4*, 367.
(52) Baranovskii, V. I.; Nikolskii, A. B. *Teor. Eksp. Khim.* **1967**, *3*, 527.
(53) Clementi, E.; Roetti, C. *At. Nucl. Data Tables* **1974**, *14*, 177.

a calculation using 75 k points in half of the zone. The other half of the zone simply yields complex conjugate wave functions that need not be calculated, but for the purposes of estimating r_0 in the above formula, $N_k = 150$. The same set of k points was used for the $H_{0.33}MS_2$ computations. For ZrS, computations for the construction of Wannier functions were carried out by using 225 k points ($N_k = 450$) spread over half of the three-dimensional Brillouin zone.

Supplementary Material Available: Extended Hückel band structure diagrams (dispersion curves) for ZrS, Mo_3S_6 (MoS_2 calculated with a $3^{1/2} \times 3^{1/2}$ supercell), MoS_2, and HMo_3S_6 ($=H_{0.33}MoS_2$). (4 pages). Ordering information is given on any current masthead page.

Contribution from the Research Laboratory of Resources Utilization, Tokyo Institute of Technology, 4259 Nagatsuta, Midori-ku, Yokohama 227, Japan

Preparation of ZnS and CdS by Thermal Degradation of (Methanethiolato)zinc and -cadmium Complexes, $[M(SMe)_2]_n$ (M = Zn, Cd)

Kohtaro Osakada* and Takakazu Yamamoto*

Received November 21, 1990

Reactions of aqueous MeSNa with $ZnCl_2$ and with $CdCl_2$ give the methanethiolato complexes $[Zn(SMe)_2]_n$ (**1a**) and $[Cd(SMe)_2]_n$ (**2**), respectively. Reaction of MeSH with $ZnEt_2$ in hexane also gives $[Zn(SMe)_2]_n$ (**1b**). $[Zn(SEt)_2]_n$ (**3**) and $[Zn(S\text{-}i\text{-}Pr)_2]_n$ (**4**) are obtained by reaction of EtSLi and *i*-PrSLi with ZnI_2, respectively. Elemental analyses of the complexes give satisfactory results. Peaks in the X-ray diffraction pattern of **1b** are considerably broader than those of **1a**. Thermolysis of **1a** and **1b** at 260 °C gives β-ZnS accompanied by evolution of MeSMe in almost quantitative yields. Thermolysis of **2** under similar conditions give CdS as a mixture of α- and β-forms. Thermogravimetric analyses of the thiolato compounds also suggest elimination of MeSMe in the vicinity of 230–240 °C. TG curves of **1b** and **2** at constant temperatures indicate that the thermolysis obeys first-order kinetics in $[M(SMe)_2]_n$. Activation parameters of the reactions are 143 and 191 kJ mol^{-1}, respectively. Thermolysis of **1a** obeys autocatalytic type kinetics expressed by the kinetic equation $\ln [x/(1 - x)] = kt + C$ (x: reacted fraction). Heating the (ethanethiolato)zinc complex **3** gives ZnS similarly to the case of **1a**, **1b**, and **2**, while thermolysis of **4** is much slower than the reactions of these complexes.

Introduction

Sulfides of several transition metals show interesting electrical and optical properties such as semiconductivity, luminescence, and photoconductivity.[1] Degradation of metal complexes with sulfur-containing ligands seems to be an attractive method for the preparation of metal sulfides because some of these complexes have sufficiently high vapor pressure or low decomposition temperature to be used as the materials for the CVD (chemical vapor deposition) process. Various transition-metal alkoxides have already been used as materials for metal oxide deposition by the MOCVD method and the sol–gel technique.[2] These procedures involve C–O bond cleavage of the alkoxide group ligating to the metal center under the reaction conditions. Since C–S bond dissociation energy is smaller than that of the corresponding C–O bond,[3] transition-metal thiolato complexes are promising as materials for metal sulfide preparation through C–S bond cleavage of the thiolato ligands.

Previously C–S bond cleavage reactions of several transition-metal thiolato complexes were reported to proceed under mild conditions.[4-9] We have also reported that bis(benzenethiolato)nickel(II) complexes having bipyridine or tertiary phosphines as auxiliary ligands gave PhSPh both in the solid state and in solution.[10]

$$Ni(SPh)_2L_2 \xrightarrow{\Delta} PhSPh \qquad (1)$$

$$L = PEt_3,\ \tfrac{1}{2}\ bpy$$

Although the metal-containing products found in (1) were mixtures of several uncharacterized compounds due to coordination of the auxiliary organic ligands to the products, yields of PhSPh were almost quantitative in the reactions. These observations suggested that degradation of homoleptic thiolato compounds of bivalent transition metals, $M(SR)_2$, would give the metal sulfides accompanied by evolution of RSR according to the equation

$$M(SR)_2 \rightarrow MS + RSR \qquad (2)$$

An ionic (thiolato)zinc complex has been reported to catalyze photodecomposition of water by using THF sacrificial reagent.[11] In the reaction ZnS, formed by partial decomposition of the complex under the reaction conditions, was responsible for the photodecomposition of water.[12]

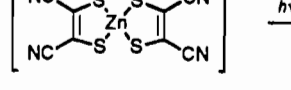

(3)

(1) (a) Henish, H. K. *Electrochemieluminescence*; Pergamon: Oxford, U.K., 1962. (b) Willardson, R. K.; Beer, A. C. *Semiconductors and Semimetals*; Academic Press: New York, 1966, 1967, 1968, 1975, and 1980; Vols. 2, 3, 4, 11, and 18. (c) Hannay, N. B. *Semiconductors*; Reinhold: New York, 1959. (d) Nag, B. R. *Electron Transport in Compound Semiconductors*; Springer: Berlin, 1980. (e) Sze, S. M. *Physics of Semiconductor Devices*; John Wiley: New York, 1981.

(2) (a) Dislich, H. *Angew. Chem.* **1971**, *83*, 428; *Angew Chem., Int. Ed. Engl.* **1971**, *10*, 363. (b) Bradley, D. C. *Chem. Rev.* **1989**, *89*, 1317.

(3) (a) Cottrell, T. L. *The Strengths of Chemical Bonds*; Academic Press: New York, 1954; p 250. (b) Benson, S. W. *Chem. Rev.* **1978**, *78*, 23.

(4) Tatsumi, K.; Sekiguchi, Y.; Nakamura, A.; Cramer, R. E.; Rupp, J. J. *J. Am. Chem. Soc.* **1986**, *108*, 1358.

(5) (a) Adams, R. D.; Yang, L.-W. *J. Am. Chem. Soc.* **1982**, *104*, 4115. (b) Adams, R. D.; Horváth, I. T.; Mathur, P.; Segmüller, B. E. *Organometallics* **1983**, *2*, 996. (c) Adams, R. D.; Horváth, I. T.; Segmüller, B. E.; Yang, L.-W. *Organometallics* **1983**, *2*, 1301.

(6) (a) Laurie, J. C. V.; Duncan, L.; Haltiwanger, R. C.; Weberg, R. T.; DuBois, M. R. *J. Am. Chem. Soc.* **1986**, *108*, 6234. (b) Birnbaum, J.; Laurie, J. C. V.; DuBois M. R. *Organometallics* **1990**, *9*, 156.

(7) Ogilvy, A. E.; Draganjac, M.; Rauchfuss, T. B.; Wilson, S. R. *Organometallics* **1988**, *7*, 1171.

(8) Ho, N. F.; Mak, T. C. W.; Luh, T.-Y. *J. Organomet. Chem.* **1986**, *317*, C28.

(9) Skripkin, Y. V.; Eremenko, I. L.; Pasynskii, A. A.; Struchkov, Y. T.; Shklover, V. E. *J. Organomet. Chem.* **1984**, *267*, 285.

(10) (a) Yamamoto, T.; Sekine, Y. *Inorg. Chim. Acta* **1984**, *83*, 47. (b) Osakada, K.; Hayashi, H.; Maeda, M.; Yamamoto, T.; Yamamoto, A. *Chem. Lett.* **1986**, 597.

(11) (a) Battaglia, R.; Henning, R.; Kisch, H. *Z. Naturforsch.* **1980**, *36B*, 396. (b) Bücheler, J.; Zeug, N.; Kisch, H. *Angew. Chem.* **1982**, *94*, 792; *Angew. Chem., Int. Ed. Engl.* **1982**, *21*, 783. (c) Zeug, N.; Bücheler, J.; Kisch, H. *J. Am. Chem. Soc.* **1985**, *107*, 1459.

0020-1669/91/1330-2328$02.50/0